

Model Predictive Energy Management for Plug-In Hybrid Electric Vehicles Considering Optimal Battery Depth of Discharge

Shaobo Xie^a, Xiaosong Hu^{b,c*}, Shanwei Qi^a, Tang Xiaolin^{b*}, Kun Lang^a, Zongke Xin^a, James Brighton^c

^a*School of Automotive Engineering, Chang'an University, Southern 2nd Road, Xi'an, 710064, China*

^b*State Key Laboratory of Mechanical Transmissions, Department of Automotive Engineering, Chongqing University, Chongqing 400044, China*

^c*Advanced Vehicle Engineering Centre, Cranfield University, Cranfield MK43 0AL, UK*

*S. Xie and X. Hu equally contributed to this research work. Corresponding authors: Emails: xiaosonghu@ieee.org and tangxl0923@cqu.edu.cn

Abstract

When developing an energy management strategy (EMS) including a battery aging model for plug-in hybrid electric vehicles, the trade-off between the energy consumption cost (ECC) and the equivalent battery life loss cost (EBLLC) should be considered to minimize the total cost of both and improve the life cycle value. Unlike EMSs with a lower State of Charge (SOC) boundary value given in advance, this paper proposes a model predictive control of EMS based on an optimal battery depth of discharge (DOD) for a minimum sum of ECC and EBLLC. First, the optimal DOD is identified using Pontryagin's Minimum Principle and shooting method. Then a reference SOC is constructed with the optimal DOD, and a model predictive controller (MPC) in which the conflict between the ECC and EBLC is optimized in a moving horizon is implemented. The proposed EMS is examined by real-world driving cycles under different preview horizons, and the results indicate that MPCs with a battery aging model lower the total cost by 1.65%, 1.29% and 1.38%, respectively, for three preview horizons (5, 10 and 15 s) under a city bus route of about 70 km, compared to those unaware of battery aging. Meanwhile, global optimization algorithms like the dynamic programming and Pontryagin's Minimum Principle, as well as a rule-based method, are compared with the predictive controller, in terms of computational expense and accuracy.

Keywords

Plug-in hybrid electric vehicle;
Energy management;
Model predictive control;
Battery Aging;
Pontryagin's Minimum Principle

Nomenclature

P_{bat}	battery power	m_f	fuel consumption
P_b	power consumed by electrical load	φ	battery purchase cost
P_l	battery internal power loss	c_f, c_e	prices of fuel fossil and electricity
P_m	motor power	SOC	initial SOC level
P_{egu}	EGU output power	SOC	final SOC level
P_{aux}	power consumed by auxiliary components	λ	co-state variable
n_m	motor rotational speed	δ	increment of initial co-state value
T_m	motor output torque	<i>List of abbreviations</i>	
Q_b	battery capacity	EMS	energy management strategy
I_b	battery electrical current	ECC	energy consumption cost
U_{oc}	battery open circuit voltage	EBLLC	equivalent battery life loss cost
R_b	battery internal resistance	SOC	battery stage of charge
Γ	nominal battery life	DOD	depth of discharge
I_{nom}	nominal battery current	MPC	model predictive control
EOL	battery end of life	PHEV	plug-in hybrid electric vehicle
σ	severity factor	DP	dynamic programming
Q_{loss}	battery capacity loss in percentage	PMP	Pontryagin's minimum principle
B	pre-exponential factor	ECMS	equivalent consumption minimum strategy
E_a	activation energy	SDP	stochastic dynamic programming
R	gas constant	AMT	automatic mechanical transmission
T	absolute temperature	HEV	hybrid electric vehicle
A_h	Ah-throughput	CD-CS	charging-depleting and charging-sustaining
z	power law factor	ISG	integrated starter generator
γ	Ah-throughput under working conditions	EGU	engine-generator-unit
t_f	duration of the trip	BSFC	brake specific fuel consumption
J	total cost	FC	fuel consumption
L	instantaneous cost	EC	electricity consumption
H	Hamilton function	RMSE	root mean squared error

1 Introduction

Low-carbon, green and sustainable development of transportation has boosted electrification of road vehicles worldwide [1]. In particular, plug-in hybrid electric vehicles (PHEVs) that are capable of improving fuel economy, enabling vehicle-grid interaction, as well as overcoming the range anxiety, have been developed and applied on a large scale [2].

For optimal economy of PHEVs, it is critical to devise an energy management strategy (EMS) for coordinating the power distribution among multiple energy sources. Many methods have been used for EMS development such as rule-based methods [3], fuzzy-logic based methods [4], optimization theory based methods like dynamic programming (DP) [5], Pontryagin's Minimum Principle (PMP) [6-7], and equivalent consumption minimum strategy (ECMS) [8-9]. Intelligent methods, e.g., machine learning [10] and artificial neural network [11-12], were also employed. For a better online application, predictive methods, especially model predictive controls, have been increasingly applied to design the EMS [13-14]. Several integrated EMSs based on two or more foregoing approaches have been also devised [15-17].

Despite the distinct improvement of battery technology in recent years, the purchase cost of a battery system still accounts for a significant proportion of overall cost of PHEV powertrains. Besides lowering the energy consumption cost (ECC), the energy management strategy is also expected to reasonably control the factors contributed to the battery aging, e.g., the depth of discharge (DOD) to extend the battery life and reduce the equivalent battery life loss cost (EBLLC), eventually minimizing the sum of the ECC and EBLLC and enhancing the life span value of vehicles. Moreover, the ECC and EBLLC are always conflicting especially for PHEVs. Typically, increased use of battery electric energy yields inexpensive propulsions and lowers the ECC; however, more battery energy depletion also indicates a deeper discharging level, which can accelerate the battery capacity fade and raise the EBLLC, probably increasing the total cost related to energy consumption and battery health decay. Therefore, when developing a sophisticated EMS, the tradeoff between the ECC and EBLLC should be carefully incorporated.

The open literature reports various methods to develop EMSs aware of battery aging. For example, for HEVs, energy management including a battery aging model was implemented based on PMP algorithm [18-19]. Control-oriented energy management was proposed to minimize fuel economy while maintaining the battery State of Health (SOH) within a reasonable range using PMP [20]. In [21], a soft constrained method was used in the EMS to optimize the power distribution between power sources, and the authors integrated a penalty term to the objective function to represent the battery life cost with respect to temperature. The ECMS was leveraged to optimize the HEV energy management considering battery aging [22]. For PHEVs, fuel economy and battery solid-electrolyte interphase (SEI) layer growth were balanced in the EMS using a stochastic DP (SDP) [23]. Moreover, SDP and particle swarm optimization (PSO) were jointly leveraged for balancing power split and battery aging for a plug-in hybrid electric city bus [24]. Further, a shortest path SDP was put forward to coordinate fuel economy and battery health [25]. The convex optimization was also proposed to simultaneously optimize the powertrain component size, state-of-health (SOH), and energy management strategy [26]. For a pure electric bus equipped with an automatic mechanical transmission (AMT), a gear-shifting strategy considering battery aging effect was constructed [27]. Also, for a hybrid energy storage system comprising batteries and ultra-capacitors, the battery durability was integrated into the development of its power distribution law [28].

It is noteworthy that the battery discharging traces (SOC profile) for charging-sustaining HEVs and plug-in HEVs are totally different. The SOC profiles of HEVs almost fluctuate around a stable level over the whole trip [19-20], whereas those of PHEVs decline from an initial value to a preset lower boundary level, e.g., 0.3 [6, 14], featuring a sloping tendency to the distance traveled. When including battery aging in the EMS, the SOC traces of HEVs are relatively stable without significant variations [19-20, 22]. For PHEVs, however, due to the clear conflict of fuel economy and battery aging, a lower boundary value of battery SOC designated in advance cannot certainly ensure minimizing the total cost; that is, a heuristically preset DOD may not guarantee the lowest total cost of ECC and EBLLC. As a result, the determination of an optimal battery DOD is critical.

Although the aforementioned EMSs of PHEVs involving battery aging take battery aging factors into account, e.g., temperature, DOD, and C-rate, they are implemented based on upper and lower boundary SOC levels assigned a priori. This treatment is mainly because the final SOC boundary is a prerequisite for solving most of the optimization algorithms, such as the conventional DP and PMP methods [5-7], where the battery DOD must be predefined. An apparent disadvantage of such a treatment is that it cannot achieve the optimal total cost of fuel economy and battery aging. Therefore, to achieve the lowest sum of ECC and EBLLC, this paper develops an EMS for PHEVs based on an optimal DOD. First, the optimal DOD targeting the minimal total cost of the energy consumption and equivalent battery aging loss is identified using PMP and a shooting method. Second, based on the optimal DOD, the SOC reference is established, and a model predictive control is further implemented to realize an online EMS. Finally, real-world speed profiles are used to examine the proposed method, and a systematic comparison with global optimization methods including DP and PMP, as well as the rule-based charging-depleting and charging-sustaining (CD-CS) method, is conducted to further demonstrate the enhanced computational accuracy and efficiency of the proposed method.

The rest of this paper is organized as follows. The PHEV modeling is formulated in Section 2, and the battery modeling is described in Section 3. The framework of the EMS is outlined in Section 4. Section 5 details the approach of determining the optimal battery DOD. Then, a model predictive control based energy management strategy is introduced in Section 6. The results and discussion are presented in Section 7, and main conclusions are drawn in Section 8.

2 PHEV Modeling

2.1 Powertrain Description

This paper considers a 12-meter long prototype plug-in hybrid electric city bus with a series configuration powertrain [14, 29], as shown in Fig. 1. The integrated starter generator (ISG) and a natural gas engine are mechanically coupled to form an engine-generator-unit (EGU). Figure 2 shows the brake specific fuel consumption (BSFC) of the engine, and Fig. 3 presents the efficiency map of the generator. The equivalent energy conversion efficiency of EGU can be calculated by combining the engine BSFC and ISG efficiency. Two electrical machines (EMs) connected with a two-level-gear reducer independently drives the wheel on either side to form a two-motor-independent system; such a system shortens the driveline and has more space available for passengers. Figure 4 shows the efficiency map of the

electric motor, which can work as a motor during driving or as a generator during braking. The maximum regenerative braking power of the motor is limited to 30 kW to avoid the extreme current impetus to the battery system. Table 1 summarizes the main specifications of the powertrain.



Fig. 1 (a) Prototype of the plug-in hybrid electrical bus [29].

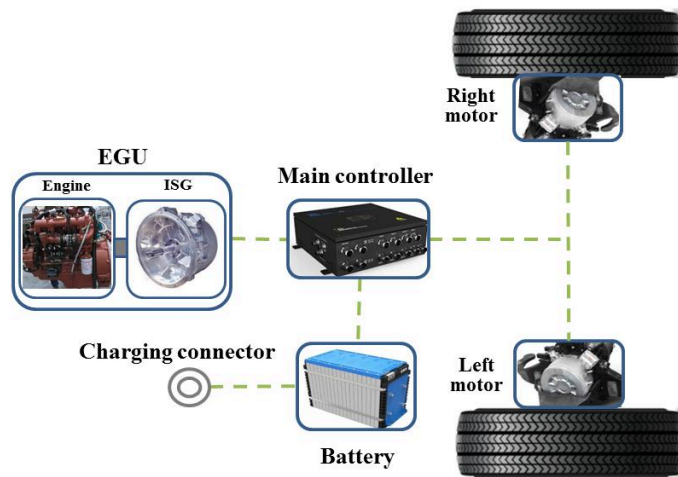


Fig. 1 (b) PHEV powertrain architecture [29].

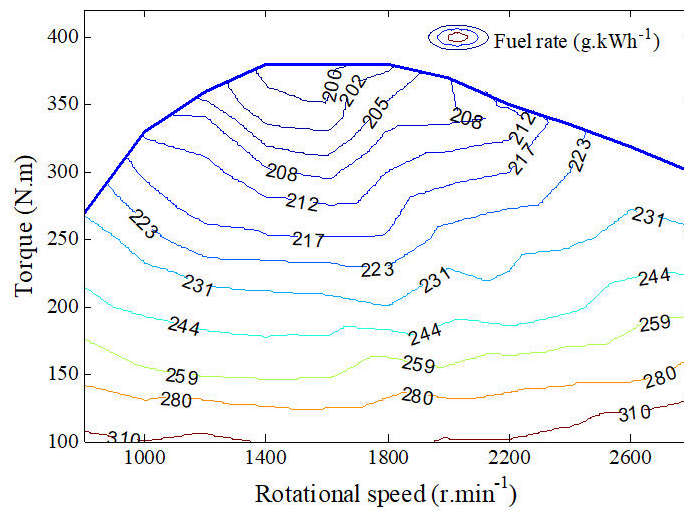


Fig. 2 BSFC of the engine [29].

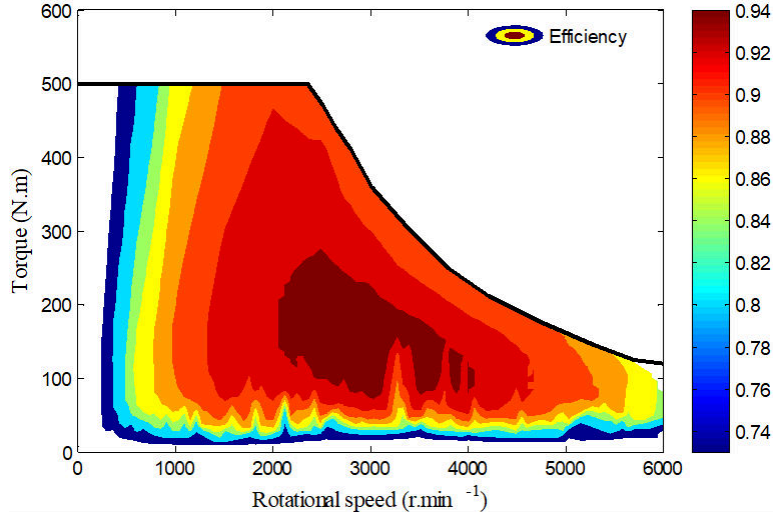


Fig. 3 Efficiency of generator [29].

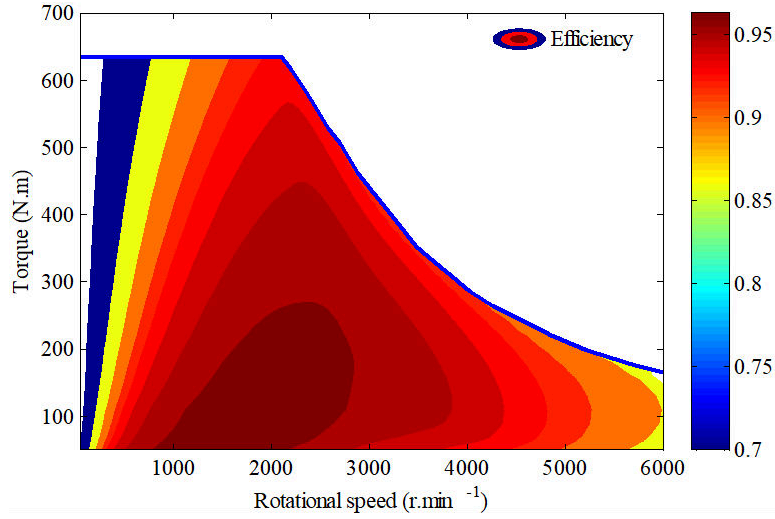


Fig. 4 Efficiency of electrical motor [29].

Table 1 Parameters of powertrain [29]

Item	Parameter	Value
Vehicle	Mass/kg	14500
	Final drive ratio	13.9
Electrical Motor	Peak power/kW	150
	Peak torque/Nm	650
	Peak speed/rpm	6000
Generator	Peak power/kW	130
	Peak torque/Nm	500
	Peak speed/rpm	6000
Engine	Displacement/L	4.2
	Peak power/kW	88
	Peak speed/rpm	2800

2.3 Vehicle dynamics

For the PHEV, the power balance equation can be written as follows:

$$\frac{1}{3600} \left(mgfv + \frac{C_d A}{21.15} v^3 + \zeta m \frac{dv}{dt} v \right) = P_{m1} \eta_{m1}^{\text{sign}(T_{m1})} + P_{m2} \eta_{m2}^{\text{sign}(T_{m2})} \quad (1)$$

$$P_b + P_{egu} = P_{m1} + P_{m2} + P_{aux} \quad (2)$$

where m is the vehicular curb mass, f is the rolling resistance coefficient; C_d is the air resistance coefficient, and A is the front area; v is the speed; ζ is the equivalent mass inertia; P_{m1} and P_{m2} are the power consumption of the left and right motors; η_{m1} and η_{m2} are electric efficiencies of the left and right motors; T_{m1} and T_{m2} are the torques of both motors. As both motors receive the same control command from the vehicular controller, we assume that they have the same output torque and electrical efficiency. P_{egu} is the EGU output power, and P_{aux} is the auxiliary power consumptions, e.g., the electrical steering system.

3 Battery Modeling

3.1 Battery Equivalent Electrical Circuit

The energy storage system is a lithium iron phosphate battery with a nominal capacity of 120 Ah and a total voltage of 537.6 V; Fig. 5 shows the equivalent electric circuit for modeling the battery dynamics. In the simulation, the open circuit voltage and equivalent internal resistance are expressed as a function of battery SOC, given that the temperature effect on battery properties is neglected [30]. For each cell, the open circuit voltage and internal resistance with respect to the SOC are shown in Fig. 6.

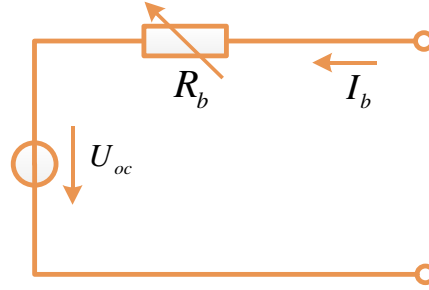


Fig. 5 Equivalent electric circuit of battery.

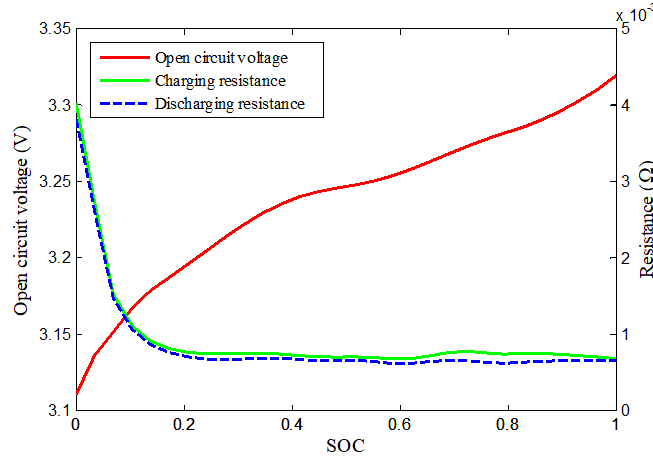


Fig. 6 Open circuit voltage and equivalent internal resistance for battery cell [29].

The power balance equation of the battery system is

$$P_{bat} = P_b + P_l = P_b + I_b^2 R_b \quad (3)$$

where P_{bat} is the total battery power, P_b is the electrical load at the terminals, and P_l is the internal loss power of the battery; I is the electrical current, and R_b is the equivalent internal resistance.

According to the power balance, the battery dynamics can be described as

$$\dot{SOC} = f(SOC) = -\frac{U_{oc} - \sqrt{U_{oc}^2 - 4R_b P_b}}{2Q_b R_b} \quad (4)$$

where Q_b is the battery capacity, and U_{oc} is the open circuit voltage.

3.2 Battery life model

This study adopts a semi-empirical battery aging model. According to the Ah-throughput model assumption, the battery nominal life is defined as in [31]

$$\Gamma = \int_0^{EOL} |I_{nom}(t)| dt \quad (5)$$

where Γ is the nominal battery life, I_{nom} is the nominal current, and EOL is the battery end of life.

Also, a severity factor to quantify the battery aging relative to nominal Ah-throughput is defined as [22]

$$\sigma = \frac{\Gamma}{\gamma} = \frac{\int_0^{EOL} |I_{nom}(t)| dt}{\int_0^{EOL} |I_b(t)| dt} \quad (6)$$

where σ is the severity factor, and γ is the Ah-throughput under working conditions.

Meanwhile, a general battery capacity loss model can be described as [32]

$$Q_{loss} = B \exp\left(\frac{-E_a}{RT}\right) (A_h)^z \quad (7)$$

where Q_{loss} is the capacity loss in percentage, B is the pre-exponential factor, E_a is the activation energy ($\text{J}\cdot\text{mol}^{-1}$), and R is the gas constant ($\text{J}\cdot\text{mol}^{-1}\cdot\text{K}$), T is the absolute temperature of lump cells (Kelvin), A_h is the Ah-throughput, and z is the power law factor.

By assuming that twenty percentage of capacity loss indicates the end of battery life, the nominal battery life Γ can be rewritten as [18-19]

$$\Gamma = \left[\frac{20}{B \exp\left(\frac{-31700 + 163.3 I_{c,nom}}{RT_{nom}}\right)} \right]^{\frac{1}{z}} \quad (8)$$

where $I_{c,nom}$ and T_{nom} are nominal battery C-rate and temperature, respectively.

Accordingly, the battery life under real load conditions can be expressed as [18]

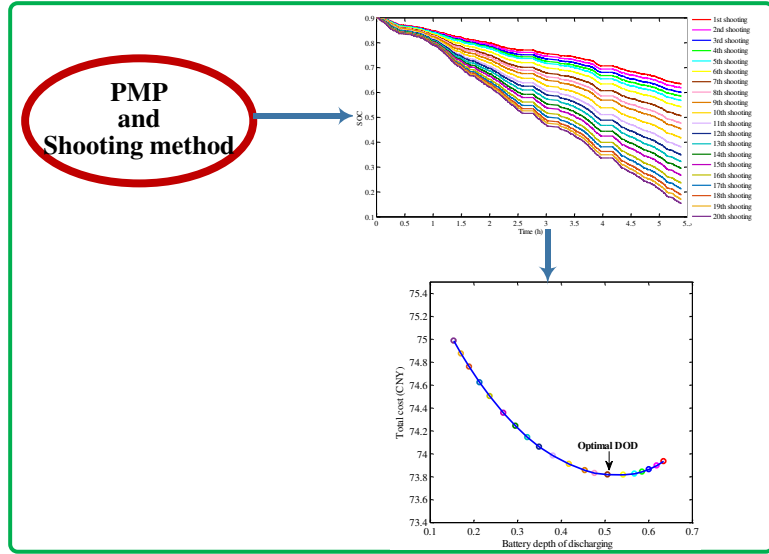
$$\gamma = \left[\frac{20}{B \exp\left(\frac{-31700 + 163.3 I_b}{RT}\right)} \right]^{\frac{1}{z}} \quad (9)$$

According to Equation (9), the temperature is one of factors on battery aging. Given that the thermal management system now has become a standard unit to cool and heat a battery pack, this study assumes a constant battery temperature of 25 °C.

4 Research Framework

The framework of the research is shown in Fig. 7. First, based on speed profiles along a city bus route, the optimal DOD can be determined by means of PMP and shooting method. Moreover, an enhanced artificial neural network forecasts the speed sequence; the network supplies the demanded power sequence and also figures out the predicted distance over the horizon for constructing the SOC reference (the justification of using this network is substantiated in comparisons with existing counterparts in Section 6.1). Then, with the optimal DOD and short-time predicted speed, the SOC reference is iteratively established, providing the battery discharging reference trace throughout the moving horizon. Finally, the DP is leveraged to acquire the local optimization solution in the preview horizon, thereby forming the model predictive control.

Optimal DOD



Model predictive control

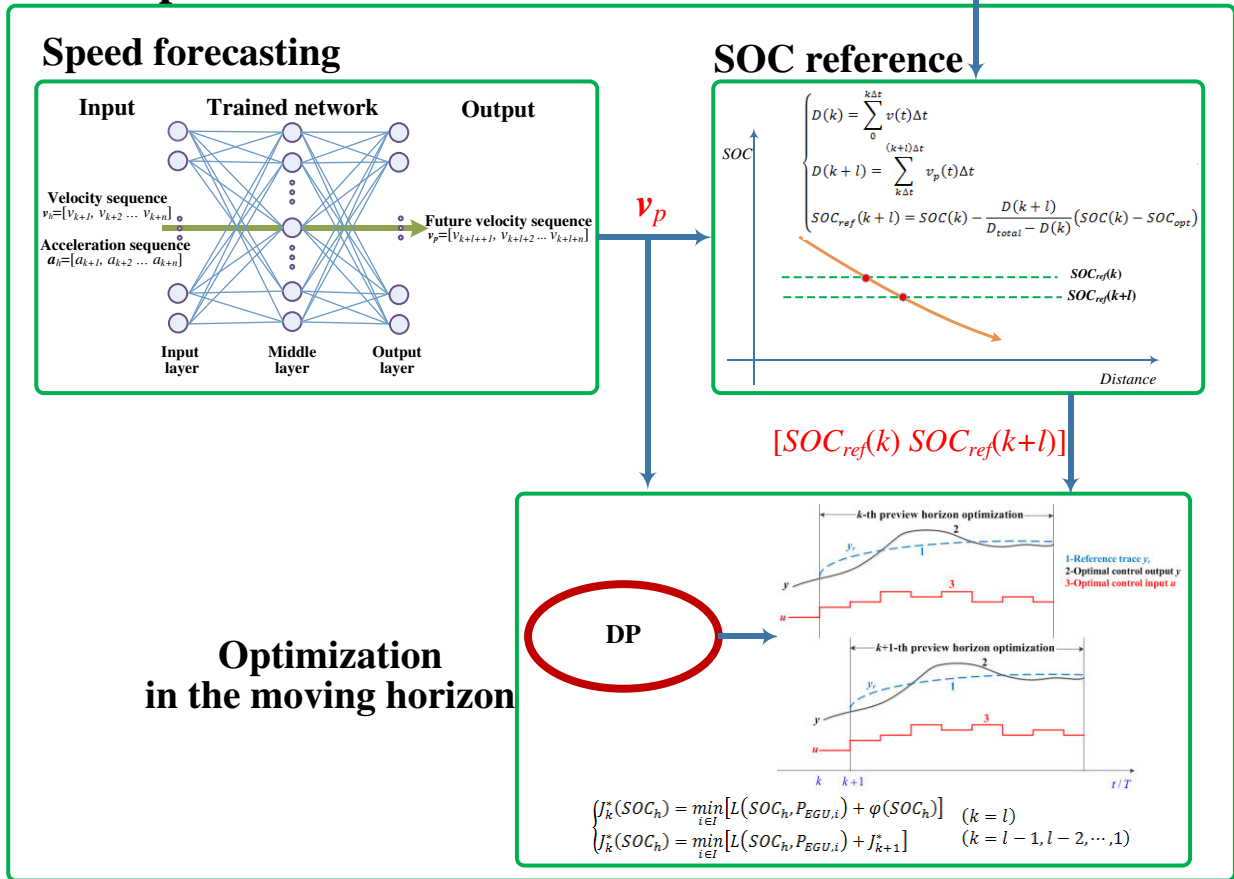


Fig. 7 Schematic of research framework.

5 Derivation of Optimal DOD

In this section, the optimal battery DOD is determined using PMP and the shooting method, so as to provide a carefully considered lower SOC boundary for the reference SOC of MPC.

5.1 PMP

The EMS concerning the battery life model seeks to minimize the sum of ECC and EBLLC. The objective function

J is defined as

$$J = ECC + EBLLC = \int_0^{t_f} L(\cdot) dt = \int_0^{t_f} \left\{ \underbrace{c_f \dot{m}_f + c_e \frac{P_{bat}}{3600}}_{ECC} + \underbrace{\varphi \sigma \frac{|I_b|}{3600\Gamma}}_{EBLLC} \right\} dt \quad (10)$$

where $L(\cdot)$ is the instantaneous total cost, and t_f is the duration of the trip; c_f and c_e are prices of fossil fuel and electricity, respectively; \dot{m}_f is the equivalent fuel rate of EGU. The battery purchase cost φ is the product of the total battery capacity and its unit price. It is worth stressing that the battery purchase cost defines EBLLC; the battery residual value is neglected when the battery reaches its end of life.

Then the Hamiltonian function H can be written as

$$H = \left(c_f \dot{m}_f + c_e \frac{P_{bat}}{3600} \right) + \varphi \sigma \frac{|I_b|}{3600\Gamma} + \lambda \dot{SOC} \quad (11)$$

where λ is the co-state variable.

Accordingly, the normal equation and co-state are given as

$$\dot{\lambda} = -\frac{\partial H}{\partial SOC} = -\lambda \frac{\partial \dot{SOC}}{\partial SOC} \quad (12)$$

and

$$\dot{SOC} = \frac{\partial H}{\partial \lambda}. \quad (13)$$

When minimizing the Hamiltonian function, the constraints of the SOC upper and lower boundaries should be met:

$$\begin{cases} \overline{SOC} = SOC_0 \\ \underline{SOC} = SOC_f \end{cases} \quad (14)$$

where \overline{SOC} and \underline{SOC} are the initial and final SOC values in the whole trip or a moving horizon.

Additionally, the physical limitations imposed by the power components are respected by

$$\begin{cases} P_{bat,min} \leq P_{bat}(t) \leq P_{bat,max} \\ P_{egu,min} \leq P_{egu}(t) \leq P_{egu,max} \\ T_{m,min} \leq T_m(t) \leq T_{m,max} \\ n_{m,min} \leq n_m(t) \leq n_{m,max} \end{cases} \quad (15)$$

where max and min represent the maximum and minimum values of the corresponding terms.

5.2 Shooting Method

This paper uses the shooting method to obtain the numerical solution of the PMP algorithm. Unlike a deterministic lower SOC boundary in [33], here the lower SOC boundary is designed to be a variable to acquire a spectrum of sums of the ECC and EBLLC for different DODs. For this purpose, the initial co-state value in each shooting changes as

$$\lambda_i = \lambda_{i-1} + \delta; \quad i = 2, 3, \dots \quad (16)$$

where i is the shooting time; λ_i is the initial co-state value, and δ is the increment of the initial co-state value in each shooting.

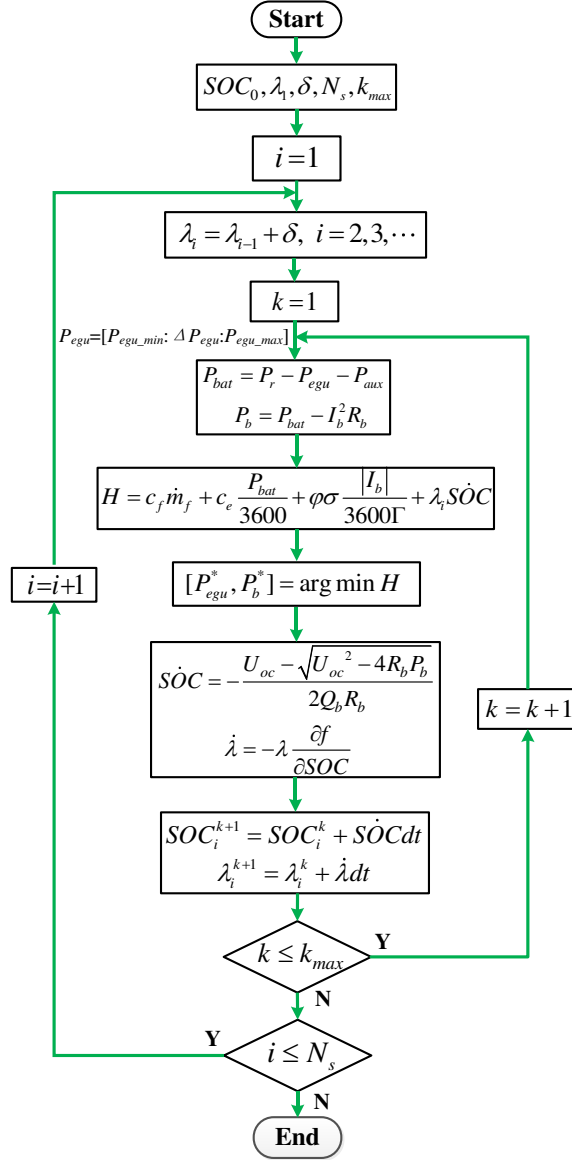


Fig. 8 Flowchart of shooting method.

Based on the shooting method, the detailed algorithmic flowchart is illustrated in Fig. 8, where i is the shooting sequence, and k is the time step of the trip with its maximum of k_{max} .

5.3 Optimal DOD

This paper considers a 70 km round-trip bus route in Xi'an, China, as a case study. Seven different speed profiles (No. 1 - No. 7) are selected randomly from the speed profiles dataset (see Fig. 9) to present the approach of capturing optimal DOD. Among them, the first six profiles (No. 1 - No. 6) are used to determine the optimal DOD, and the last one to examine the proposed method (see Section 7). These bus cycles were used in our previous work [14].

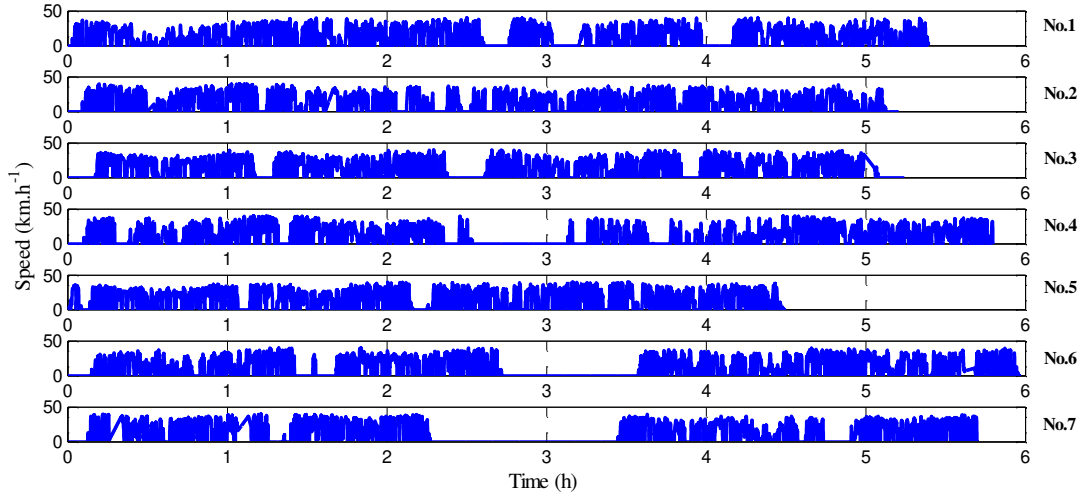


Fig. 9 Speed profiles along a city bus route [14].

The main parameters for the numerical solution of the PMP method are specified as follows. The prices of the natural gas and electricity are set to 3.8 CNY.L^{-1} and 0.8 CNY.kWh^{-1} , respectively. The battery unit purchase cost is assumed to be $1400 \text{ CNY.kWh}^{-1}$, so that the total purchase cost of the battery system is approximately 90300 CNY. The initial co-state value λ_0 and the increment δ are set to -1.6 and 0.1, respectively; N_s , which controls the shooting times, is set to 20 to guarantee a sufficient number of points to accurately identify the optimal DOD. According to [19], the gas constant R is set to $8.31 \text{ J.mol}^{-1}\text{.K}$, T is set to 298.16 K, the power exponent z is specified as 0.57, and the pre-coefficient B is approximately set to 4650.

The speed profile No.1 is taken as an example to demonstrate the process of determining the optimal DOD. By using the shooting method with a free lower SOC boundary, the SOC profiles can be yielded accordingly (see Fig. 10), where each battery DOD determines ECC and EBLLC, and thus a total cost. Figure 11 shows the curve of the total cost with respect to DOD. The total cost features an approximate upward Para-curve, where lower or higher DODs lead to an increased total cost. Clearly, when DOD reduces from its optimal value to lower levels, e.g., 0.2, to pursue improved fuel economy, the total cost grows at a faster pace. In this way, the optimal DOD corresponding to the minimum total cost can be achieved; the initial co-state value is shown in Fig. 12 accordingly.

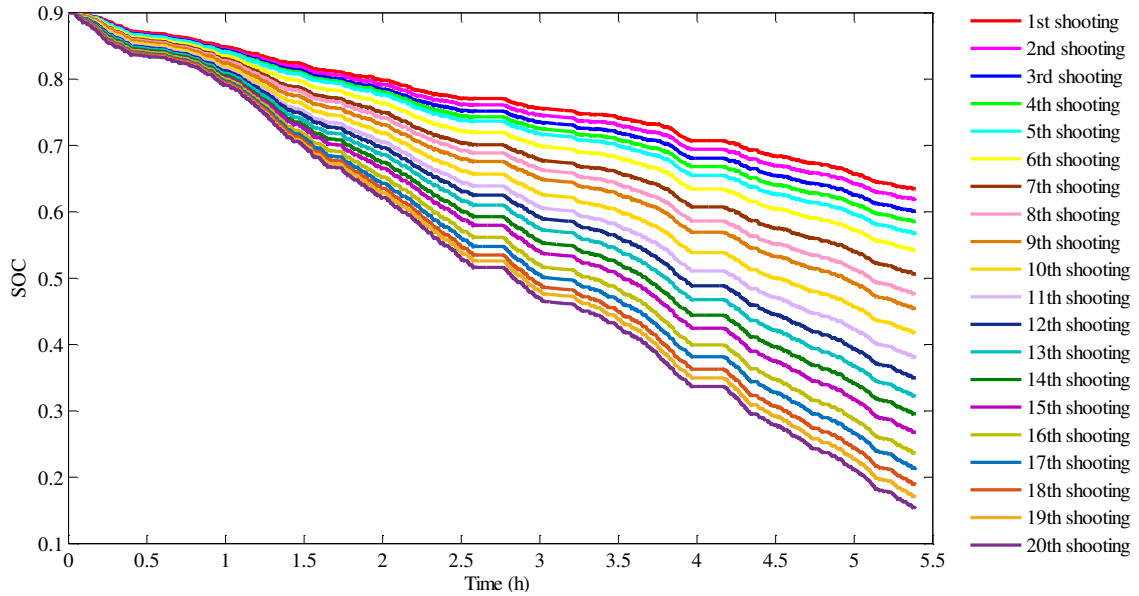


Fig. 10 SOC profiles in the shooting method.

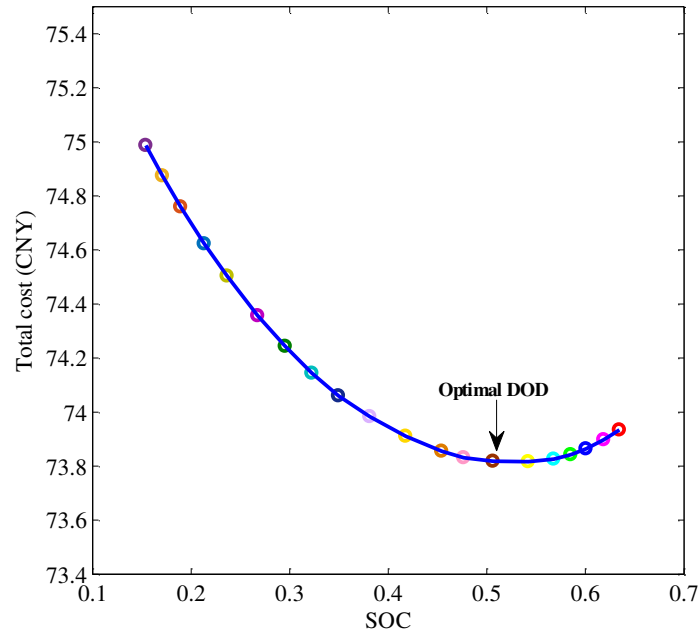


Fig. 11 Total cost versus the battery DOD.

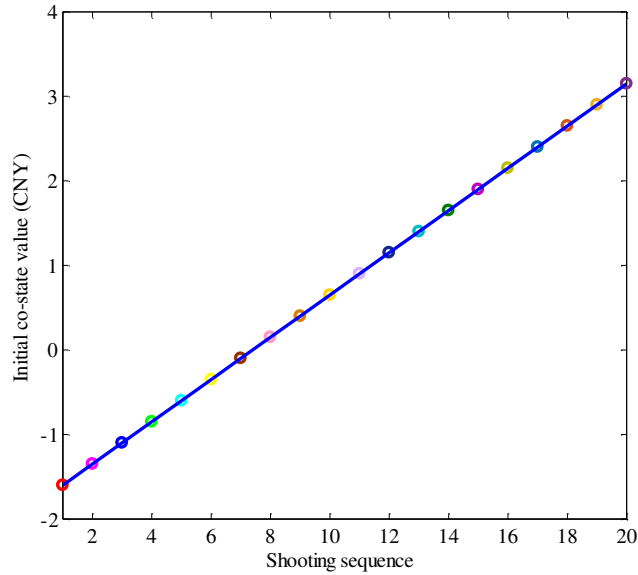


Fig. 12 Initial co-state values over the shooting sequence.

Table 2 summarizes the calculated fuel consumption (FC), electricity consumption (EC), EBLLC, total cost, and optimal DOD for the six speed profiles. The optimal DOD maintains around 0.51, with slight differences among different trips. This behavior can be explained by considering that despite relatively stable traffic environment for the city bus route, the speed profiles still deviate from one another due to many random factors, resulting in a minor difference of the optimal DOD. Nonetheless, the optimal DOD, overall, still can be specified to a fixed value, i.e., the mean level (0.51) for the running cycles (No. 1 - No. 6).

Table 2 Results of different speed profiles

Speed profile number	FC(L)	EC(kWh)	EBLLC(CNY)	Total cost(CNY)	Optimal DOD
No.1	8.85	24.23	20.81	73.82	0.5184
No.2	8.37	24.23	20.27	71.46	0.5194
No.3	9.63	23.86	20.02	75.71	0.5243
No.4	9.13	23.71	20.50	74.16	0.5265
No.5	8.64	25.37	20.37	73.50	0.5019
No.6	9.08	24.97	20.32	74.80	0.5072

6 MPC

With the optimal DOD, this section develops a model predictive control based EMS, in which the local optimization is solved in the moving horizon to trade-off the battery aging and fuel economy.

6.1 Speed Forecasting

To optimize the power distribution over the moving horizon, a short-time speed sequence should first be forecast to obtain the power sequence. Here a back-propagation artificial neural network (BPANN) is used to realize the speed forecasting. To explore the potential of the speed forecasting method, BPANN with a single input (speed sequence), BPANN with two inputs (both speed and acceleration sequences), and a Markov chain model are comprehensively compared. The forecasting accuracy and computational time are summarized in Table 3. It is evident that BPANN with both speed and acceleration sequences as inputs has the best accuracy among the three methods, despite a reduction of computational efficiency. In order to improve the accuracy of the controller, the BPANN with two inputs is chosen as the speed predictor, without a sacrifice of real-time implementability. Figure 13 presents the architecture of a common three-layer neural network that includes the input layer, hidden layer, and output layer. The inputs of BPANN are the historical speed and acceleration sequences $\mathbf{v}_h=[v_{k+1}, v_{k+2}, \dots, v_{k+n}]$ and $\mathbf{a}_h=[a_{k+1}, a_{k+2}, \dots, a_{k+n}]$, and the output is the future short-time speed sequence $\mathbf{v}_p=[v_{k+l+1}, v_{k+l+2}, \dots, v_{k+l+n}]$. Here, No. 1 - No. 6 speed profiles are used once again for the neural network training while No. 7 is used for the neural network examination. All the calculations are conducted on a desktop computer with the CPU main frequency of 3.4 GHz and a memory of 16 GB. Table 4 summarizes the neural network properties.

Table 3 Comparison of different speed forecasting methods

Preview horizon length (<i>l</i>)	BPANN (single input)		BPANN (two inputs)		Markov chain model	
	RMSE (km.h ⁻¹)	Computational time per horizon (s)	RMSE (km.h ⁻¹)	Computational time per horizon (s)	RMSE (km.h ⁻¹)	Computational time per horizon (s)
5s	2.02	0.0108	1.33	0.0109	1.87	0.0005
10s	4.70	0.0111	3.90	0.0114	4.63	0.0016
15s	7.00	0.0118	5.90	0.0127	6.53	0.0038

Note: RMSE means the root-mean-square error of the forecast speed.

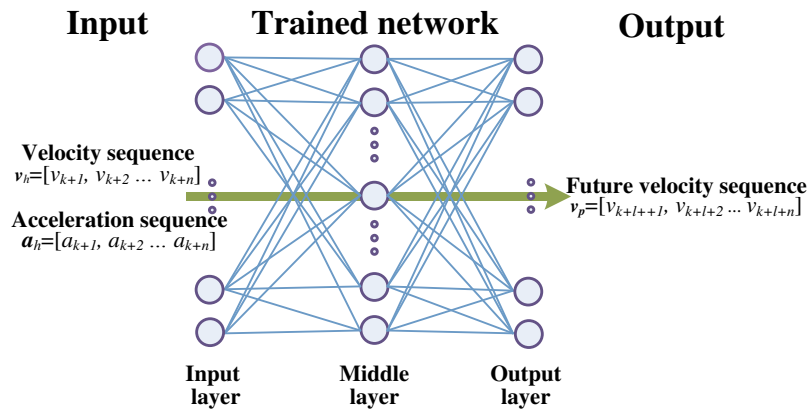


Fig. 13 Structure of artificial neural network.

Table 4 Neural network properties

Item	Value
Number of hidden layer nodes	10
Iterative times	10
Learning ratio	0.1
Learning target	0.00004
Activation function	$(1 - e^{-x})^{-1}$

The investigation considers three preview time horizon lengths of 5, 10 and 15 s. Figure 14 compares the forecast and real speeds within a time interval 2.36 - 2.64 h for the three time horizons. It is clear that the forecast speed matches well the reference for the preview horizon of 5 s, with a RMSE of 1.33 km.h⁻¹. RMSEs for the preview horizons of 10 and 15 s increase to 3.90 and 5.90 km.h⁻¹, respectively, due to a weak causal link between the input historical and forecasting sequences over a longer preview horizon.

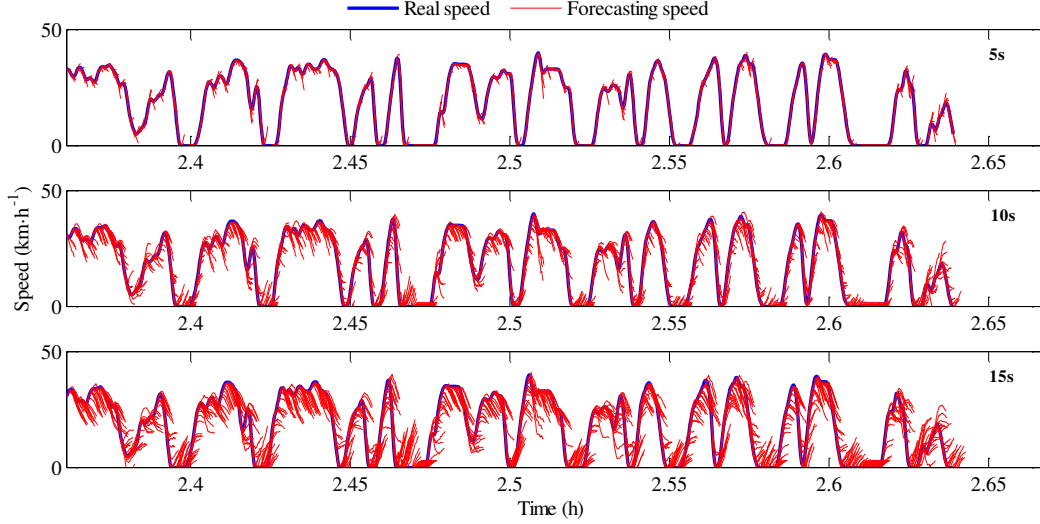


Fig. 14 Comparison between real and forecasting speeds.

6.2 SOC Reference

For the MPC based EMS, to solve the local optimization over the moving horizon, a SOC reference with the lower and upper boundary SOC's have to be carefully specified in each prediction horizon for implementing the optimization algorithm. Here an iterative SOC reference is chosen [14],

$$\begin{cases} D(k) = \sum_0^{k\Delta t} v(t)\Delta t \\ D(k+l) = \sum_{k\Delta t}^{(k+l)\Delta t} v_p(t)\Delta t \\ SOC_{ref}(k+l) = SOC(k) - \frac{D(k+l)}{D_{total} - D(k)}(SOC(k) - SOC_{opt}) \end{cases} \quad (17)$$

where k is the time index, and l is the preview horizon length; v and v_p are real and forecasting speeds, respectively; $D(k)$ is the distance travelled up to the k th step, and $D(k+l)$ is the forecasted driving distance in the preview horizon; $\Delta t = 1$ s is the time interval. D_{total} is set to 71 km. Meanwhile, SOC_{opt} corresponds to the optimal DOD and is specified to 0.51 as indicated in Section 5.3.

6.3 Dynamic Programming in Moving Horizon

This paper uses the DP method to solve the local optimization over the preview horizon, for the sake of simplicity and efficacy. In the k th predictive horizon the discrete DP can be formulated as:

$$\begin{cases} J_k^*(SOC_h) = \min_{i \in I} [L(SOC_h, P_{EGU,i}) + \varphi(SOC_h)] & (k = l) \\ J_k^*(SOC_h) = \min_{i \in I} [L(SOC_h, P_{EGU,i}) + J_{k+1}^*] & (k = l-1, l-2, \dots, 1) \end{cases} \quad (18)$$

where J is the cost-to-go value, l is the prediction horizon length, SOC_h is h th discrete element in its allowable set, and $P_{EGU,i}$ is i th delivered EGU power in the allowable set I . Further, $\varphi(SOC_h)$ is a penalty function imposed to restrain an excessive discharge of the battery, which has the form of [5],

$$\varphi(SOC_h) = \begin{cases} 0 & SOC_h \geq SOC_{ref}^k \\ \alpha(SOC_h - SOC_{ref}^k)^2 & SOC_h < SOC_{ref}^k \end{cases} \quad (19)$$

where α is a constant, which is set to 10^5 , and SOC_{ref}^k is the lower boundary of SOC reference determined by (17). Meanwhile, for the local optimization problem, the physical constraints for the power components described as in (15) must be satisfied.

7 Results and Discussion

For common EMSs with a preset DOD, the lower SOC boundary is expected to reach a lower allowable target, e.g., 0.2, to improve fuel economy, because the battery electrical energy can yield less expensive propulsion than fossil fuels. Therefore, the proposed method with the optimal DOD and cases with a preset lower SOC boundary (0.2), are compared to further evaluate the proposed approach.

As described in Section 6.1, speed profiles from No. 1 - No. 6 are used for speed forecasting, and No. 7 is used to validate the proposed method. The conventional DP and PMP methods that can produce a global optimal solution, as well as the rule-based CD-CS strategy, are also used to examine the MPC. Table 5 summarizes the results of different methods.

For the methods related to the DP algorithm, i.e., the conventional DP method and MPC with the DP algorithm acquiring local solution in each prediction horizon, the computational accuracy and expense are affected by the SOC discretization scale, due to considerable interpolation calculations to estimate the cost-to-go. Higher discretization scale can improve the solution accuracy to some degree, but unavoidably increase the computational time. For a fair comparison with other methods, the number of discrete SOC points in each horizon for MPC is set to 10, and for the conventional DP over the whole trip is set to 300.

The results highlight that the methods using a battery life model induce smaller total costs than those without it. Precisely, MPC schemes with a battery life model cut the total cost down by 1.23, 0.96, and 1.02 CNY or 1.65%, 1.29% and 1.38% for the preview horizons of 5, 10, and 15 s, respectively, compared to MPCs unaware of battery aging. Moreover, a comparison between the two types of MPCs suggests that the one including battery life model consumes almost 230% more fossil fuel and 44% less electric energy, resulting in a smaller EBLLC for battery longevity. On the contrary, MPCs unaware of battery aging consume more electricity and less fossil fuel, leading to a higher EBLLC.

Compared to the global methods (DP and PMP) that produce virtually the same total cost, MPCs have a slightly increased total cost, because they essentially base a local optimization solution over moving horizons. Also, compared to the CD-CS strategy, the proposed MPCs cut down the total cost by more than 10.1 CNY or 12.2%.

As for computational burden, Table 5 reveals that the rule-based CD-CS method has the best time efficiency. For both global methods, the DP method is more time-consuming than the PMP method. For MPCs, a growing preview horizon length expands the computational time, because the local optimization solved by the DP method over a longer prediction horizon needs heavier calculation expense. Moreover, while the MPC-15s is most time-consuming among the three MPCs, its average computational time per preview horizon is less than 0.086 s, which satisfies the requirement of real-time applications.

Table 5 Results of different methods with and without the battery life model

Method	Battery life model	FC (L)	EC (kWh)	EBLLC (CNY)	Final SOC	Total cost (CNY)	Time per drive cycle (s)
MPC-5s	With	8.67	25.94	20.94	0.5097	74.64	590
MPC-10s		8.77	25.45	20.78	0.5171	74.47	1249
MPC-15s		8.56	25.77	21.02	0.5121	74.16	1867

PMP	Without	8.95	25.57	20.36	0.5138	74.01	58
DP		8.91	24.69	20.39	0.5283	74.03	2312
MPC-5s		2.62	46.95	28.36	0.1892	75.87	570
MPC-10s		2.70	46.10	28.29	0.2022	75.43	1239
MPC-15s		2.50	46.30	28.64	0.1992	75.18	1853
PMP		3.27	44.10	27.11	0.2010	74.83	59
DP		2.77	45.99	27.82	0.2036	75.14	2189
CD-CS		5.50	43.33	29.20	0.2449	84.76	18

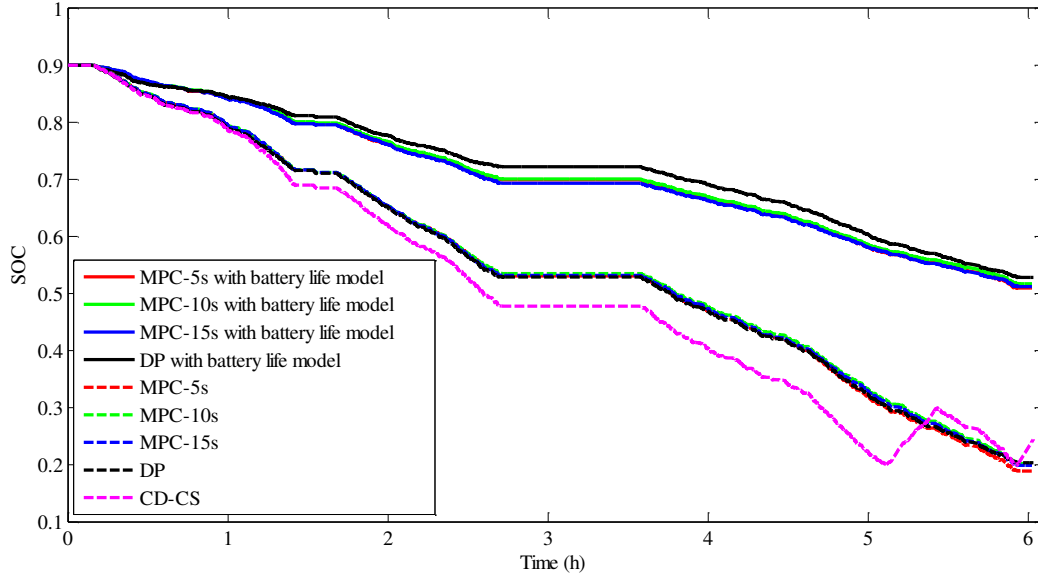


Fig. 15 SOC profiles of different methods.

Figure 15 plots the SOC profiles of the foregoing methods. The slope of SOC profiles with the battery life model is not as steep as those without the battery life model, indicating the influence of the battery aging model. Also, the SOC profiles of MPCs are close to those of the DP and PMP methods, which reveals similar electric energy consumption. For the rule-based strategy, the charging-depleting state first takes place, followed by the charging-sustaining state with the SOC fluctuating between 0.2 and 0.3, which induces the largest total cost.

As the city bus route features low average speeds and demanded power, the advantage of the proposed EMS considering battery longevity is not fully displayed. In scenarios with higher average speed, accompanied by larger electric current fluxes in and out of the battery frequently, the battery life model will be used more to protect the battery aging and lead to more obvious decrease of the total cost, compared to EMSs without battery health perception.

8 Conclusions

This paper proposes a novel predictive energy management scheme of PHEVs considering the optimal battery DOD to minimize the total cost related to both fuel economy and equivalent battery life loss. The PMP and shooting method are used to show the trend of the total cost for different SOC boundary values, and a knee point corresponding to the minimum total cost can be found to determine the optimal DOD. Based on the optimal DOD, a SOC reference is prepared for the moving horizon optimization, and then the MPC is implemented with real speed profiles. The proposed method is compared with the DP, PMP, as well as the rule-based CD-CS method, in terms of computational accuracy and time. The results indicate that the proposed MPC can significantly reduce the equivalent battery life loss cost and thus the total cost, compared to counterparts without a battery aging model. Moreover, quantitative results reveal that the proposed MPC reduces the total cost by 1.65%, 1.29% and 1.38%, respectively, for three preview horizons (5, 10 and 15 s), in contrast to cases unconscious of battery aging. And the MPC with a battery aging model can decrease the total cost by more than 12.2% for the three preview horizons, compared to the CD-CS method. The average computational time per a moderate preview horizon (e.g., 5s) is less than 0.086 s, displaying a great potential of real-time implementation.

The future research will extend the methodology of identifying the optimal depth of battery discharge for electrified vehicles in the context of the vehicle-to-vehicle and vehicle-to-infrastructure.

Acknowledgements

This work was supported in part by the EU-funded Marie Skłodowska-Curie Individual Fellowships (IF) Project under Grant 706253-pPHEV-H2020-MSCA-IF-2015, and in part by the Fundamental Research Funds for the Central Universities of China (Grant no. 310822151026, 310822151121, 106112016CDJXZ338825, 106112017CDJQJ338811) and National Natural Science Foundation of China (Grant no. 51875054).

References

1. T. Liu, X. Hu, S. Li, D. Cao. Reinforcement learning optimized look-ahead energy management of a parallel hybrid electric vehicle, *IEEE/ASME Transaction on Mechatronics*, 2017, 22(4): 1497-1507.
2. Martinez C M, Hu X, Cao D, Velenis E, Gao B, Wellers M. Energy Management in plug-in hybrid electric vehicles: recent progress and a connected vehicles perspective. *IEEE Transactions on Vehicular Technology*, 2017, 66(6):4534-4549.
3. Gonder J, Markel T. Energy management strategies for plug-in hybrid electric vehicles. *SAE Technical Paper*, 2007, no. 2007-01-0290.
4. Schouten N J, Salman M A, Kheir N A. Fuzzy logic control for parallel hybrid vehicles. *IEEE Transaction on Control System Technology*, 2002, 10(3): 460-468.
5. Liu J, Peng H. Modeling and control of a power-split hybrid vehicle. *IEEE Transactions on Control Systems Technology*, 2008, 16(6): 1242-1251.
6. Onori S, Tribioli L. Adaptive Pontryagin's minimum principle supervisory controller design for the plug-in hybrid GM Chevrolet Volt. *Applied Energy*, 2015, 147: 224-234.
7. Xie S, Hu X, Xin Z, Brighton J. Pontryagin's minimum principle based model predictive control of energy management for a plug-in hybrid electric bus. *Applied Energy*, 2019, 236: 893-905.
8. Serrao L, Onori S, Rizzoni G. ECMS as a realization of Pontryagin's minimum principle for HEV control. *American Control Conference*, 2009: 3964-3969.
9. Sun C, Sun F, He H. Investigating adaptive-ECMS with velocity forecast ability for hybrid electric vehicles. *Applied Energy*, 2017, 185: 1644-1653.
10. Xiong R, Cao J, Yu Q. Reinforcement learning-based real-time power management for hybrid energy storage system in the plug-in hybrid electric vehicle. *Applied Energy*, 2018, 211: 538-548.
11. Tian H, Lu Z, Wang X, Zhang X, Huang Y, Tian G. A length ratio based neural network energy management strategy for online control of plug-in hybrid electric city bus. *Applied Energy*, 2016, 177: 71-80.
12. Xie S, Hu X, Qi S, Lang K. An artificial neural network-enhanced energy management strategy for plug-in hybrid electric vehicles. *Energy* 2018, 163: 837-848.
13. Xie S, Hu X, Liu T, Qi S, Lang K, Li H. Predictive vehicle-following power management for plug-in hybrid electric vehicles. *Energy*, 2019, 166: 701-714.
14. Xie S, Hu X, Xin Z, Li L. Time-efficient stochastic model predictive energy management for a plug-in hybrid electric bus with adaptive reference state-of-charge advisory. *IEEE Transaction Vehicle Technology*, 2018, 67(7): 5671-5682.
15. Chen Z, Xiong R, Wang C, Cao J. An on-line predictive energy management strategy for plug-in hybrid electric vehicles to counter the uncertain prediction of the driving cycle. *Applied Energy*, 2017, 185: 1663-1672.
16. Zhang F, Liu H, Hu Y, Xi J. A supervisory control algorithm of hybrid electric vehicle based on adaptive equivalent consumption minimization strategy with fuzzy PI. *Energies*, 2016, 9: 919.
17. Chen Z, Mi C C, Xu J, Gong X, You C. Energy management for a power-split plug-in hybrid electric vehicle based on dynamic programming and neural networks. *IEEE Transactions on Vehicular Technology*, 2014, 63(4): 1567-1580.
18. Suri G, Onori S. A control-oriented cycle-life model for hybrid electric vehicle lithium-ion batteries. *Energy*, 2016, 96: 644-653.
19. Tang L, Rizzoni G, Onori S. Energy management strategy for HEVs including battery life optimization. *IEEE Transactions on Transportation Electrification*, 2015, 1(3): 211-222.
20. Ebbesen S, Elbert P, Guzzella L. Battery state-of-health perceptive energy management for hybrid electric vehicles. *IEEE Transactions on Vehicular Technology*, 2012, 61(7): 2893-2900.
21. Padovani T M, Debert M, Colin G, Chamailard Y. Optimal energy management strategy including battery health through thermal management for hybrid vehicles. *IFAC Proceedings Volumes*, 2013, 46(21): 384-389.
22. Serrao L, Onori S, Sciarretta A, Guezennec Y, Rizzoni G. Optimal energy management of hybrid electric vehicles including

- battery aging. American Control Conference, 2011: 2125-2130.
23. Moura S J, Stein J L, Fathy H K. Battery-health conscious power management in plug-in hybrid electric vehicles via electrochemical modeling and stochastic control. *IEEE Transactions on Control Systems Technology*, 2013, 21(3): 679-694.
 24. Wang Y, Jiao X, Sun Z, Li P. Energy management strategy in consideration of battery health for PHEV via stochastic control and particle swarm optimization algorithm. *Energies*, 2017, 10(11): 1894.
 25. Xu F, Jiao X, Wang Y, Jing Y. Battery-lifetime-conscious energy management strategy based on SP-SDP for commuter plug-in hybrid electric vehicles. *IEEJ Transactions on Electrical and Electronic Engineering*, 2018, 13(3): 472-479.
 26. Hu X, Martinez C M, Yang Y. Charging, power management, and battery degradation mitigation in plug-in hybrid electric vehicles: A unified cost-optimal approach. *Mechanical Systems and Signal Processing*, 2017, 87: 4-16.
 27. Liu T, Zou Y, Liu D. Energy management for battery electric vehicle with automated mechanical transmission. *International Journal of Vehicle Design*, 2016, 70(1): 98-112.
 28. Zhang S, Xiong R, Sun F. Model predictive control for power management in a plug-in hybrid electric vehicle with a hybrid energy storage system. *Applied Energy*, 2017, 185: 1654-1662.
 29. Wang J, Xie S, Liu X, Yuan Y, Li B, Li S. Research and development of a chassis for the extended-range and plug-in commercial vehicle. Shaanxi automobile Group Research Report, 2015. (In Chinese)
 30. Johnson V H. Battery performance models in ADVISOR. *Journal of power sources*, 2002, 110(2): 321-329.
 31. Marano V, Onori S, Guezennec Y, Rizzoni G, Madella N. Lithium-ion batteries life estimation for plug-in hybrid electric vehicles. *Vehicle Power and Propulsion Conference, IEEE-VPPC*, 2009: 536-543.
 32. Bloom I, Cole B W, Sohn J J, Jones S A, Polzin E G, Battaglia V S, et al. An accelerated calendar and cycle life study of Li-ion cells. *Journal of Power Sources*, 2001, 101(2): 238-247.
 33. Xie S, Li H, Xin Z, Liu T, Wei L. A Pontryagin minimum principle-based adaptive equivalent consumption minimum strategy for a plug-in hybrid electric bus on a fixed route. *Energies*, 2017, 10(9): 1379-1399.

2019-02-22

Model predictive energy management for plug-in hybrid electric vehicles considering optimal battery depth of discharge

Xie, Shaobo

Elsevier

Xie S, Hu X, Qi S, et al., (2019) Model predictive energy management for plug-in hybrid electric vehicles considering optimal battery depth of discharge. *Energy*, Volume 173, April 2019, pp. 667-678
<https://doi.org/10.1016/j.energy.2019.02.074>

Downloaded from Cranfield Library Services E-Repository